Accepted Manuscript

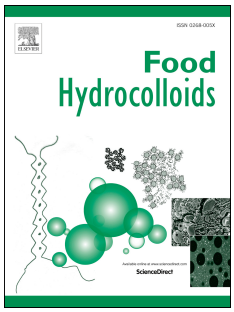

Effect of acid hydrolysis on the multi-scale structure change of starch with different amylose content

Pei Chen, Fengwei Xie, Lei Zhao, Qian Qiao, Xingxun Liu

PII: S0268-005X(16)30997-3

DOI: 10.1016/j.foodhyd.2017.03.003

Reference: FOOHYD 3814

To appear in: *Food Hydrocolloids*

Received Date: 12 December 2016

Revised Date: 10 February 2017

Accepted Date: 1 March 2017

Please cite this article as: Chen, P., Xie, F., Zhao, L., Qiao, Q., Liu, X., Effect of acid hydrolysis on the multi-scale structure change of starch with different amylose content, *Food Hydrocolloids* (2017), doi: 10.1016/j.foodhyd.2017.03.003.

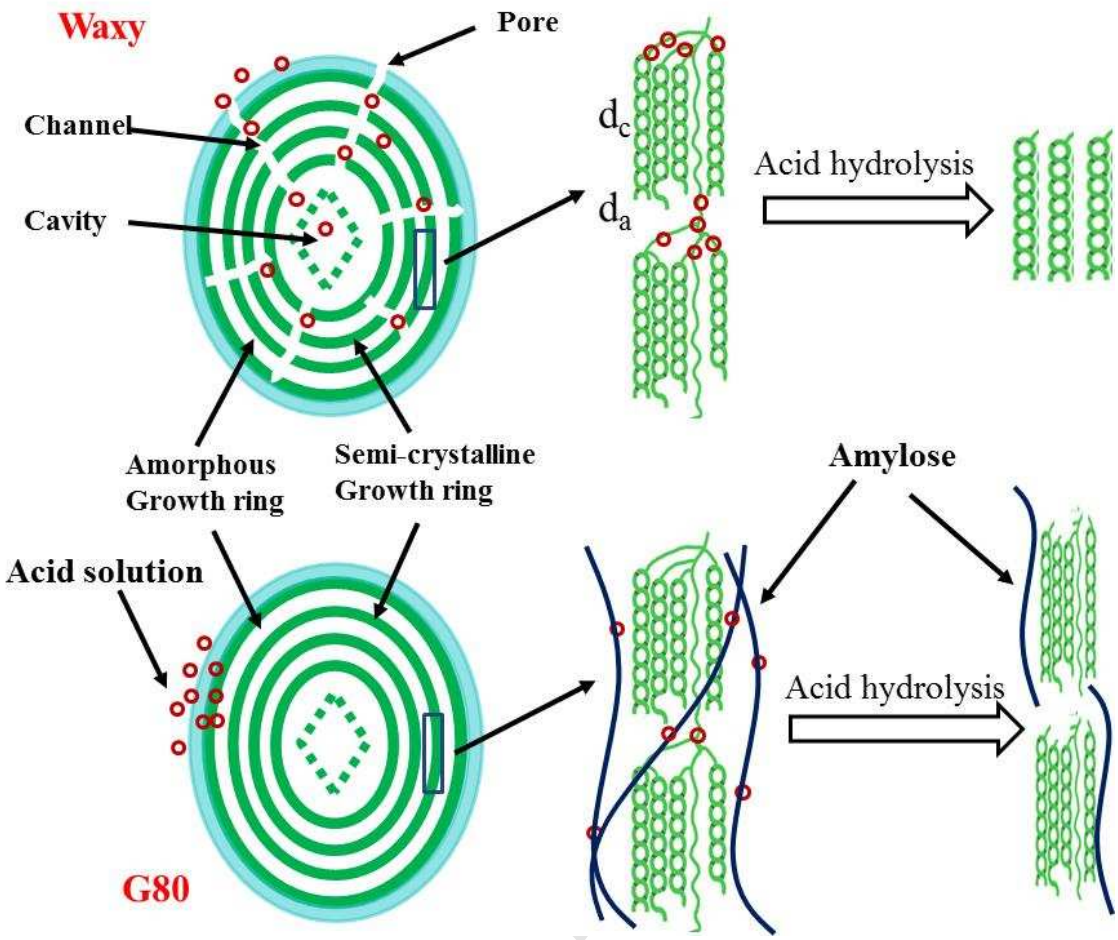

Effect of acid hydrolysis on the multi-scale structure change of starch with different amylose content

Pei Chen[a]*, Fengwei Xie[b], Lei Zhao[a], Qian Qiao[a], Xingxun Liu[c]**

[a] School of Food Science, South China Agricultural University, Guangzhou 510642, China

[b] School of Chemical Engineering, The University of Queensland, Brisbane, Qld 4072, Australia

[c] Institute of Food Science and Technology (IFST), Chinese Academy of Agricultural Science (CAAS), Beijing, 100193, China

* Corresponding author at: School of Food Science, South China Agricultural University, Guangzhou, China. *E-mail*: peichen@scau.edu.cn (P. Chen)

** Corresponding author at: Institute of Food Science and Technology, CAAS, Beijing, China. *E-mail:* ytboy652@163.com (X. Liu).

Abstract:

This work demonstrates how the multi-scale structure of starch granules changes during acid hydrolysis. The degradation mechanism has also been discussed. Both the whole native Gelose 80 (G80) starch in its granule form and the enzyme debranched G80 starch degraded apparently until a stable size was reached. In contrast, no degradation of the debranched waxy starch was observed from size exclusion chromatography (SEC) results. This indicated that amylose and amylopectin were hydrolyzed through cleavage of α-(1→4) and α-(1→6) linkages, respectively. From X-ray diffraction (XRD), the relative crystallinity was increased with increased acid treatment days. Small-angle X-ray scattering (SAXS) results showed that the lamellar peak intensity and crystalline thickness (d_c) from 1D correlation function for G80 were increased during acid hydrolysis. However, the lamellar structure of waxy starch disappeared quickly. Using scanning electron microscopy (SEM) and confocal laser scanning microscopy (CLSM), two different acid hydrolysis patterns were observed at the starch granule level including the endo-corrosion pattern in waxy starch and the exo-corrosion pattern in G80. Those differences would lead to the quick degradation of the lamellar structure of waxy starch and contributed to the gradual crystallinity increase for G80 starch. Thermal degradation behavior from thermogravimetric analysis (TGA) results showed that the thermal decomposition temperature of acid-hydrolyzed starch was shifted to low temperature, which confirmed the molecular weight degradation during acid hydrolysis. This work enables a further understanding of acid hydrolysis mechanism, which is of value for the acid processing of starch-based foods.

Keywords: Starch, Acid hydrolysis, amylose and amylopectin, lamellar, granule organization

1. Introduction

Starch is not only the main component of food providing a vital energy for humans but also used in food industry as the food additives such as gelling agents, thickeners, emulsion stabilizers and fat replacers to improve the food quality. Recently, starch is attracting much attention for edible or biodegradable materials due to its advantages of biodegradability and low costs (Liu, et al., 2016). For example, starch or starch-gelatin blends have been developed for use as medical capsule materials (Zhang, et al., 2012; Zhang, et al., 2013). The multi-scale structure of starch determines the thermal (Li, et al., 2016), rheology (Xie, et al., 2009) and nutritional properties (Xu, et al., 2017), which in turn affect characteristics of food products. Thus, the understanding of the structure changes during processing is a fundament issue to design desired starch-based foods.

Acid hydrolysis of native starch is an important modification method used in the starch industry to prepare thin boiling starches to improve the viscosity or conversion extent, and is widely used in food, paper, textile and other applications (Wang, Truong, & Wang, 2003). Recently, starch nanoparticles prepared by acid hydrolysis to enhance mechanical and barrier properties of biodegradable nanocomposites have attracted much attention (Jiang, Liu, Han, Xiong, & Sun, 2016; Le Corre, Bras, & Dufresne, 2010). The acid concentration, type and hydrolysis time may affect the microstructure and function properties of starch. For example, the degradation of amylose and amylopectin at a high acid concentration can result in a decrease in storage modulus (G′), loss modulus (G″), gelling temperature, and gel strength of the acid-thinned starches (Wang, et al., 2003). Compared with single acid modification, combined modification methods are widely used to change the starch structure and functionality, especially for the formation of resistant starch. For instance, acid hydrolysis together with hydrothermal modifications may benefit the formation of resistant starch (Zavareze & Dias, 2011). Moreover, acid hydrolysis with autoclaving and subsequent β-amylolysis could significantly reduce the starch digestibility (Song, Janaswamy, & Yao, 2010). These combined modification methods would further extend industrial

applications of modified starches in food and materials.

Acid hydrolysis has been proved to be an efficient approach in improving the understanding of the starch granule structure (Chen, et al., 2009; Wang, Blazek, Gilbert, & Copeland, 2012). Acid hydrolysis is considered to yield the resistant crystalline parts of the granule, which allows the estimation of the easily degradable fraction and the amorphous part of the starch. The preferential hydrolysis of amorphous regions, which are mainly composed of central amorphous areas and peripheral amorphous growth rings, results in an increase in the relative proportion of crystalline regions and double helices (Wang & Copeland, 2015). The hydrolysis kinetics shows two stages during the hydrolysis process. In the first rapid stage, the amorphous layers within the starch granule are assumed to be eroded, and in a second slower stage, the crystallites are degraded (Gérard, Colonna, Buléon, & Planchot, 2002; Genkina, Kiseleva, & Noda, 2009). Both amylose and amylopectin are located on the surface of the granules and are attacked simultaneously in the early stages of acid hydrolysis.

Many papers have reported the effect of acids hydrolysis time on the starch structure and functional properties. However, to the best of our knowledge, there are no paper systematically reporting on the changes of the starch multi-scale structure during acid hydrolysis. In this study, two maize starches, which are rich in amylose (G80) and amylopectin (waxy), respectively, were used as model materials to reveal the mechanism of acid hydrolysis of starch. The multi-scale structure of starch involves the molecular and lamellar structures and the granule, which were studied by SEC, XRD, SAXS, and CLSM, respectively. The information obtained from this study would help to understand the acid degradation mechanism and to design new starch materials with accurately-controlled structures.

2. Material and Method

2.1 Materials

Waxy maize starch (waxy) and high-amylose maize starch (Gelose 80, or G80)

were purchased from Penford Australia Pty Ltd. (Lane Cove, NSW, Australia). Waxy and G80 have amylose/amylopectin ratios of 2/98 and 80/20, respectively, as measured using the iodine colorimetric method. 8-amino-1, 3, 6-pyrenetrisulfonic acid (APTS), sodium cyanoborohydride and HCl acid are chemically pure and purchased as received from Sigma-Aldrich Corporation.

2.2 Preparation of acid-hydrolyzed starch

Native starches (waxy and G80) were suspended in 2M HCl (15 g of dry starch per 300 ml). The container was sealed with a lid and kept at room temperature (20 °C) for 12 days, and the mixtures were gently shaken daily to re-suspend the precipitated granules. Then, samples were taken after different days and centrifuged at 4000 RPM for 15 min. The residue was washed with distilled water until the filtrates was at neutral pH and then were dried at 40 °C overnight under an air stream.

2.3 Scanning Electron Microcopy (SEM)

The preparation of starch granules for SEM observation was according to the previous method (Chen, et al., 2009). In order to observe the inner structure of starch, A few starch granules were embedded in epoxy and then poured into a tube mound. After cured overnight at room temperature, these starch granules set in epoxy were held in liquid nitrogen for 3 min and cryo-fractured for imaging. The sections were then immersed in 2 mol/L HCl solution at room temperature for different days, following which the sections were then rinsed three times for ten minutes each time with distilled water. These sections were dried at room temperature overnight under an air stream.

A scanning electron microscope (X230, Philips, Eindhoven, Netherlands) was used to investigate the appearance and surface of the starches. The samples were coated with iridium in a vacuum evaporator and viewed in the SEM at a low accelerating voltage of 2 kV.

2.4 Confocal Laser Scanning Microscopy (CLSM)

Native and hydrolyzed starch samples were prepared for CLSM as previously described (Blennow, et al., 2003; Chen, et al., 2011). Starch granules (10 mg) were dispersed in 15 µL of freshly-made APTS solution (10 mM APTS dissolved in 15% acetic acid), and 15 µL of 1M sodium cyanoborohydride was added. The reaction mixture was incubated at 30°C for 15-18 h, with the granules washed 5 times with 1 ml of distilled water and finally suspended in 20 µl of 1:1 (v/v) glycerol/water mixture. A drop of the mixture was then mounted on a glass plate for microscopy.

A confocal laser scanning microscope equipped with an Ar/Hg laser (TCS SP2, Leica Microsystems, Wetzlar, Germany) with a stand for fixed fluorescent cell samples was used to investigate the internal morphologies of the starches. The Leica objective lens used were 60x Plan-Apo/1.40 oil UV. During image acquisition, each line was scanned four times and averaged to reduce the noise.

2.5 X-Ray Diffractions (XRD)

Wide-angle X-ray diffraction (WAXD) traces of starch granules were studied by a Bruker D8 Diffractometer operating at 40 kV and 40 mA, with Cu Kα radiation monochromatized with a graphite sample monochromator. Before the analysis, the moisture content of all the samples was adjusted to ~10% by drying at 40 ºC for 24 h. Relative crystallinity (RC) of the samples was quantitatively estimated by measuring the peak area of crystallinity following the method described before (Pei Chen, et al., 2016; Z. Li, et al., 2016). The intensity was measured from 2 to 40° as a function of 2θ and at a scanning speed of 2°/min.

2.6 Small-angle X-ray scattering (SAXS)

Synchrotron small-angle X-ray scattering (SAXS) measurements were carried out at the BL16B1 beamline at the Shanghai Synchrotron Radiation Facility (SSRF), China. Distilled water was added to the starch to obtain a starch suspension with the starch: water ratio being 1:3 (w/v) in a glass vial and equilibrated for 24 h before the SAXS tests. Then, the starch suspension (0.70 mL) was loaded into 2-mm-thick sample cells, of which the front and back windows were both covered with the Kapton

tape. Two-dimensional (2D) Mar165 were used to collect the 2D SAXS patterns. The wavelength of the incident X-ray was 1.24 Å and the sample-to-detector distance (SDD) was 1940 mm for SAXS measurements. A beef tendon specimen was used as standard materials for the calibration of the scattering vector of SAXS. By measuring sample adsorption using the ionization chambers in front and back of the sample cell, we performed data correction, calibrated the SAXS data from the background scattering, and normalized the data on the primary beam intensity. Background subtraction follows the equation:

$$I_s(\theta) = I_t(\theta) - \frac{I_t}{I_b}\frac{T_t}{T_b}I_b(\theta).$$

$I_t(\theta)$, $I_b(\theta)$ and $I_s(\theta)$ represent the distribution of scattering intensity of samples held in cells, sample cells and pure samples, respectively. I_t and I represent values of samples held in the cells and sample cells, read from the ionization chambers in front of sample cell. T_i and T_t represent the transmissivity of the samples held in cells and sample cells.

The normalized 1D correlation function $\gamma_1(r)$ is defined as

$$\gamma_1(r) = \int_0^\infty I(q)q^2\cos(qr)dq / Q$$

where $\underline{I}(q)$ is scattering intensity, q is scattering vector defined as $q = 4\pi\sin\theta/\lambda q$ (2θ is the scattering angle) and r is the direction along the lamellar stack. Because of the finite q range of experimental SAXS data, extrapolation of the 1D SAXS data to both the low and high q ranges are necessary for the integration of the intensity, $I(q)$. Extrapolation to low q was performed using an intensity profile based on Guinier's law, and the extension of the intensity to large q values can be accomplished using the Porod-Ru land model (Kuang, et al., 2017; Yang, Liang, & Han, 2015; Yang, Liang, Luo, Zhao, & Han, 2012). The parasitic scattering and thermal fluctuation were corrected using a normalized 1D correlation function.

2.7 Size-exclusion chromatography

The molecular size and size distribution of fully-branched and debranched starch molecules were measured using size-exclusion chromatography (SEC) (Tran, et al.,

2011). The extracted native starch granules (about 6 mg) were dissolved in DMSO/LiBr solution and then debranched using isoamylase in acetate buffer (pH ~3.5), following the method of Li et al. (Li, Hasjim, Dhital, Godwin, & Gilbert, 2011). Then, the weight size distributions of fully-branched and debranched starch molecules were analyzed in duplicate using SEC (Agilent 1260 series, Agilent Technologies) equipped with a refractive index detector (Optilab T-rEX, WYATT Corp., USA). The injection volume was 100 μL, the flow rate was 0.3 mL/min, and the column oven temperature was at 80 °C. A series of columns (GRAM precolumn, GRAM 30, and GRAM 3000 analytical columns, Polymer Standard Services, Mainz, Germany) were used to analyze the size distribution of fully-branched starch molecules, and another series of columns (GRAM precolumn, GRAM 100, and GRAM 1000 analytical columns, Polymer Standard Services, Mainz, Germany) was used to analyze the size distribution of debranched starch molecules. A series of pullulan standards (Polymer Standard Services, Mainz, Germany) with varying molecular weights ranging from 342 to 2.35×10^6 Da were used for the calibration to obtain the relation between the SEC elution volume and the hydrodynamic volume V_h (which is the separation parameter for SEC). Data are presented as the SEC weight distribution, $w(\log V_h)$, as a function of the corresponding hydrodynamic radius R_h, with $V_h = (4/3)\mathrm{Pi}R_h^3$. Because the largest standard had a hydrodynamic radius of ~ 50 nm, this is the maximum size at which calibration was reliable. The dependence of R_h on the elution volume for larger sizes was obtained by the extrapolation of the calibration curve and thus were only semi-quantitative, and also sensitive to day-to-day variations (Wang, Hasjim, Wu, Henry, & Gilbert, 2014).

2.8 Thermogravimetry (TGA)

A Pyris-1 TGA apparatus was used to study the thermal decomposition of samples heated to 650 °C at a rate of 20 °C/min in air condition.

3. Result and Discussion

3.1 Change in molecular size distribution of whole (fully-branched) starch

It is well known that starch mainly consists of amylopectin, a highly-branched glucan molecule (~10^8 Da), and amylose, a linear glucan molecule (~10^6 Da) with few long branches. Fig.1 shows the molecular size distributions of whole acid-hydrolyzed starch with different times. Here, all the weight distributions of the whole starch molecules were normalized to the highest peak. Generally, for normal maize starch with amylose content of 25%, two peaks were observed from SEC. One peak (R_h < 100 nm) was due to the amylose and the other (100 nm < *Rh* < 5,000 nm) was due to the amylopectin.

From Fig.1, It could be seen that the size distribution of fully-branched starch became narrow and shifted to a lower molecular size with the increased acid hydrolysis time, which meant that both waxy and G80 starches were degraded during acids hydrolysis. For the native and acid-hydrolyzed waxy starch, no discernible amylose peak was observed. However, in the native waxy starch, a shoulder with the size of amylose, R_h = 10~100 nm was observed. This shoulder could be due to the amylose (about 2%), or the partially shear degraded amylopectin molecules, which had a similar hydrodynamic size to amylose, and hence co-eluted during the SEC analysis (Teng, Witt, Wang, Li, & Hasjim, 2016). However, this shoulder disappeared after acids hydrolysis, even within a short time (2 Days). Moreover, for the degraded amylopectin molecules, a new peak (R_h = 6~8 nm) was observed, representing the stable size achieved during acid hydrolysis. This phenomenon was reported to be observed in the *in-vitro* digestion cooked starch (Teng, et al., 2016) and the extruded starches (Witt, Gidley, & Gilbert, 2010), although the size of those enzyme-resistant starch (R_h ~ 2.5 nm) was smaller than the acid-hydrolyzed starches. For the G80 starch, a much less distinct distribution between amylose and amylopectin was shown. R_h of G80 was also decreased from 30 nm to 5 nm with the increased acid hydrolysis time, which was similar to the case of waxy maize starch.

Both waxy and G80 starches degraded quickly within the first two days and degraded very slowly between 4 to 6 days. This trend was consistent with a previous study of the hydrolysis kinetics by determining the content of soluble sugar in the

solution or the recovery yield of insoluble starch (Kim, Lee, Kim, Lim, & Lim, 2012; Wang, et al., 2015). The acid hydrolysis kinetics of starch exhibited a two-stage hydrolysis pattern, a fast initial rate and a slower subsequent rate (Kim, et al., 2012). The former was considered corresponding to the hydrolysis of the amorphous parts while the latter was due to the simultaneous hydrolysis of the amorphous and crystalline regions (Wang, et al., 2012).

3.2 Chain length distribution of starch molecules

The weight molecular size distributions of the debranched starch from the native and acid-hydrolyzed starches were normalized to yield the same height of the highest peak (Fig. 2). For the native starch, the first peak (1.5 nm < R_h < 4 nm) indicated the amylopectin branches spanning over one lamella (A and B_1 chains), the second peak (4 nm < R_h < 6 nm) represented the amylopectin branches that were confined to more than one lamella (B_2, B_3, ... chains), and the remaining broad peaks (6 nm < R_h < 100 nm) were due to the amylose branches (Kuang, Xu, Wang, Zhou, & Liu, 2016; Teng, et al., 2016; Wu, Morell, & Gilbert, 2013). For the waxy starch, there were no qualitative differences in the molecular size distributions of the short amylopectin branches (1.5 nm < R_h < 4 nm), the same phenomenon has been found in Naegeli dextrins (H. Jiang, Srichuwong, Campbell, & Jane, 2010) . However, the proportions of long amylopectin branches (4 nm < R_h < 6 nm) were decreased after 2 and 4 days of acid hydrolysis. For the high amylose starch (G80), the amylose chains were degraded very quickly after acid hydrolysis, then kept to a stable size of R_h about 3.5 nm, which was higher than that for the waxy starch (R_h ~2.5 nm).

3.3 Change in crystalline structure

Fig.3 shows the XRD patterns of the native and acid hydrolyzed starches investigated. It can be seen that the waxy starch showed the typical A-type pattern, with strong reflections at 2θ of about 15°, 17°, 18° and 23°, with an unresolved big doublet between 17° and 20°. G80 showed the strongest diffraction peak at 2θ of around 17° and a few small peaks at 2θ of 5.6°, 20° and 22°, as well as an additional

peak, appeared at about 5.6°. These spectra were characteristic of the B-type pattern (Frost, Kaminski, Kirwan, Lascaris, & Shanks, 2009; Li, et al., 2016).

From Fig.5, it could be seen that the native and acid hydrolyzed starches displayed the same pattern. The diffractions peak seemed more clear after acid hydrolysis. The change in the degree of crystallinity was shown in Fig.6. As expected, the proportion of crystallinity in both waxy and G80 starches increased with the increased acid hydrolysis time, which meant that the acid degraded the amorphous parts preferentially. However, initially, the degree of crystallinity for the waxy starch was increased faster than for G80 starch. This is as expected as the waxy starch was more susceptible to acid hydrolysis whereas high-amylose starch has more compact structure which is more resistant to external attacks.

3.4 Change in lamellar structure

SAXS is a non-destructive and efficient method to study the lamellar structure of starch, which measures the variations in electron density distributions of amorphous and crystalline lamellae in the granule starch (Blazek & Gilbert, 2011). Fig.5 shows the double-logarithmic SAXS patterns of the native and acid-hydrolyzed starches. A typical scattering peak at ca. 0.06 $Å^{-1}$ was observed in the SAXS curves for the native waxy and G80 starch, which was corresponding to the 9-10nm semi-crystalline lamellar structure of starch (Kuang, et al., 2017). From Fig. 5, it can be clearly seen that the scattering intensity of the lamellar peak for the waxy starch was higher than for the G80 starch. This indicated that the waxy starch had a higher electron density contrast ($\Delta\rho = \rho_c - \rho_a$, where ρc and ρa are the electron densities of the crystalline regions and the amorphous regions in the semi-crystalline lamellae) between crystalline and amorphous lamellae.

The scattering intensity of lamellar peak for the acid-hydrolyzed waxy starch decreased quickly after the treatment for 2 days. Afterward, the lamellar peak disappeared with further acid hydrolysis. Compared with the waxy starch, G80 showed the opposite trends. Acid hydrolysis increased the scattering intensity of the lamellar peak for the high amylose starch. The lamellar peak remained even after

acids hydrolysis for 8 days.

Recently, the 1D correlation function is widely used in the analysis of starch lamellar structure and provides basic structure parameters such as the thickness of crystalline (d_c), amorphous (d_a) region of the lamella and long period distance (d_{ac}= d_a+d_c) (Chen, et al., 2016; Fan, et al., 2013; Yang, et al., 2016). The detailed method has been described before (Goderis, Reynaers, Koch, & Mathot, 1999; Kuang, et al., 2017). The normalized 1D correlation function can be seen in Fig.6, where we assigned the larger layer thickness to the amorphous and crystalline thickness. Since the lamellar peak for the waxy starch disappeared after acid hydrolysis for more than 2 days, the 1D correlation function cannot be applied in this curve.

Fig.7 shows the changes in d_c, d_a, and d_{ac} for the G80 starch with acids hydrolysis. From Fig.7, it could be seen that the long period distance (d_{ac}) from the correlation function was increased at first, then kept stable. A significant decrease in d_a and an increase in d_c with the increased acids hydrolysis time could be clearly observed.

3.5 Change in granules structure

Fig.8 shows the SEM images of the waxy and G80 starches after acid hydrolysis for different days. All the starch granules showed a mixture of the rounded and angular granule. The waxy starch granule usually contained four or five sides, while the G80 starch had some three-sided and small irregular pieces. Both waxy and G80 starch granules did not show significant changes from the native forms after 2 days of acid treatment. However, a few small cracks were appearing on the surface in the waxy starch. With further acid hydrolysis, both waxy and G80 starches showed surface degradation by exo-corrosion. It should be noticed that endo-corrosion also occurred in the waxy starch (Fig.8 c and Fig.8 e). This was as expected as the center of the waxy starch granule (hilum) is most vulnerable to acid hydrolysis (Wang, et al., 2012). The central area of the granule around the hilum is believed to be the least organized region of the starch granule (Wang, et al., 2012), where amylopectin had more longer long B-chains (Jane, Wong, & McPherson, 1997; Pan & Jane, 2000).

Endo-corrosion was not observed for the G80 starch granules, which only showed roughened surface.

The inner structure of starch by acid hydrolysis was also observed using SEM (see Fig.8). It can be clearly seen that the sizes of internal cavities in the waxy and G80 starch granules were increased with the increased acid hydrolysis time. While the growth rings were not visible under SEM cross-section images for the native starch granules, for waxy starch these rings became gradually clearer with the increased acid hydrolysis time. However, for the G80 starch, the growth rings were not observable even after acid hydrolysis for 6 days.

Using CLSM after the fluorescence labeling with APTS, the appearance of internal cavities in the starch granules could also be identified (see Fig.8). The channels were visible as dark lines running from the border of the granule toward the hilum in the waxy starch granules, which has been reported previously (Huber & BeMiller, 2000; Kim & Huber, 2008). The APTS fluorescence intensity for the G80 starch was greater than that for the waxy starch. Regarding this, compared with amylopectin, amylose is a much smaller molecule and contains a much higher molar ratio of reducing ends per anhydrous glucose residue. This could result in a higher by-weight labeling of amylose (Blennow et al., 2003). After acid hydrolysis, stronger fluorescence could be seen, which meant that acid hydrolysis led to an increased number of reactive ends, which reacted with more APTS molecules. The same phenomenon has been observed by Chung and Lai (Chung & Lai, 2006).

3.6 Thermal decomposition

Fig.9 shows the thermal decomposition of the native and acid hydrolyzed waxy and G80 starches studied by TGA under air conditions. The derivative mass loss curves are shown in the right corner, where the decomposition stages were presented as peaks. Our previous work (Liu, et al., 2014; Liu, et al., 2013; Liu, Yu, Liu, Chen, & Li, 2008, 2009; Liu, et al., 2010) has shown that the heating condition may affect the thermal decomposition behavior of starches. In particular, the dehydration and decomposition are two separate processes, which can be observed clearly during the

thermal degradation of starch in an inert condition, such as N_2. Here, in the air condition, the thermal decomposition of starches could be observed with three decomposition steps. The first step is observed below 150 °C, which was related to the evaporation of the free moisture in starch. The second stage was from 250 to 375 °C, with the mass decreased dramatically, which was similar to the thermal degradation procedure in an inert condition. The third stage was next to the second stage and finished at about 600 °C. This region was termed ‘‘glowing combustion’’, which produced simple gasses such as CO, CO_2, and H_2O due to the reactions of carbonaceous residues with oxygen.

The TGA results here showed that the thermal decomposition temperature of the acid-hydrolyzed waxy and G80 starches were lower than their native counterparts. This was in accordance with the GPC results showing the decreased molecular weights.

3.7 Mechanism of acid degradation of maize-starches

The acids hydrolysis of native starch is an important modification method used in the starch industry as it is effective to change the inner structure and functional properties of starch without disrupting its granule morphology (S. Wang, et al., 2015). Moreover, acid hydrolysis is also an important way to reveal the starch granule structure. A thorough understanding of the acid hydrolysis mechanism particularly regarding the most important factors controlling the starch structure and functionality will increase the knowledge in starch scientific research and industrial applications

It is well known that the acid hydrolysis of starch follows a few steps (see Fig.10). Firstly, the acid penetrates into the starch granule, with the preferential attacking on the granule surface. Then, the acid erodes the loosely-packed amorphous regions in the starch granule and degrades the starch molecules (Qiao, et al., 2016). The preferential hydrolysis of the amorphous regions results in an increase in the relative crystallinity.

Our results here showed that the acid hydrolysis of the waxy starch was faster than that of the G80 starch. The efficiency of acid hydrolysis at the granule level

could be influenced by the porosity of starch granules (Huber & BeMiller, 1997; Huber, et al., 2000). With the pores in the waxy starch granules, the acid solution could hydrolyze the granules from the inside towards the periphery. However, the G80 starch was hydrolyzed from the surface towards the interior of granules, with the diffusion of the acid into the granules at a rather slow rate. The difference between the endo-corrosion pattern for the waxy starch and the exo-corrosion pattern for the G80 starch would be due to the surface features of the starch granule. In particular, the presence of pores and channels in the waxy starch granules allowed the acid to penetrate towards the less-organized granule interior, which was in contrast to the rigid and smooth surface of the waxy starch and the interior of the G80 starch (Dhital, Warren, Zhang, & Gidley, 2014). This was in agreement with our previous study (Chen, et al., 2009), where the CLSM results confirmed that the waxy starch had clear internal cavities and channels, while the G80 one had bright cores.

The starch aggregation structures, including the crystalline and amorphous lamellar structure, and the double helices arrangement and packing in the lamellar structure, also affect the acid hydrolysis (Gérard, et al., 2002; S. Wang, et al., 2012). It is well known that the acid preferentially hydrolyzes the amorphous parts in starch granules, which results in a higher proportion of crystallinity. With the endo-corrosion pattern for the waxy starch, the lamellar structure disappeared quickly, and the crystallinity was decreased quickly at first. In contrast, the exo-corrosion of the G80 starch could only act through a “washing” procedure from the peripheral regions of the granules, which caused gradual decreases in the lamellar structure and crystallinity.

Acid hydrolysis would cause the degradation of both amylose and amylopectin, which was confirmed by SEC. Compared with the hydrolysis by α-amylase which shows specificity for α-(1→4) linkages, a hypothesis of the cleavage of α-(1→6) branch points by acid hydrolysis have been reported (S. Wang, et al., 2012; S. Wang, et al., 2015). From the SEC results, the whole waxy starch showed a fast degradation, while the enzyme debranched waxy starch showed mild degradation. Therefore, acid hydrolysis might be acting mainly on the α-(1→6) branch point. However, the G80

starch was also degraded by acid treatment, which meant that α-(1→4) linkages were also degraded. For the waxy starch, the α-(1→6) branch points always existed in the amorphous regions. Thus, the cleavage of α-(1→6) branch points could increase the amylose content (as tested by the Con A binding method (Wang, et al., 2012; Wang, et al., 2015)) and the crystallinity. For the G80 starch, the degradation of amylose molecules in the amorphous regions increased d_c (also decreased d_a). Regarding this, the acid treatment might have reduced the amorphous zone, swollen the crystalline zone within lamellae. However, the free amylose chains caused by acid cleavage of some of the amylose molecule might contribute to the formation of new crystal structure. The thermal degradation temperature of the acid-treated starch was shifted to lower temperatures also agreed with the degradation of the starch molecular weight.

4. Conclusion

The present investigation focuses on the changes of the starch multi-scale structure during acid hydrolysis. The degradation mechanism of acid hydrolysis has also been explored. The molecular, aggregation and granule structures were studied by SEC, XRD, SAXS, SEM, and CLSM from nanometer to micrometer, respectively. The SEC results showed that the whole native starch (waxy and G80) molecules and the debranched native G80 starch were degraded obviously to a stable size, while the degradation of the debranched native waxy starch was not significant. This phenomenon indicated that amylose and amylopectin were hydrolyzed through cleavage of α-(1→4) and α-(1→6) linkages, respectively. The relative crystallinity from XRD was increased with the increased acid treatment time. Acid hydrolysis also increased the lamellar peak intensity and d_c from the 1D correlation function for the G80 starch. However, the lamellar structure of the waxy starch disappeared quickly. Two different acid hydrolysis patterns at the granule level were observed, including the endo-corrosion pattern for the waxy starch and the exo-corrosion pattern for the G80 starch.

With the known information of the starch granule structure, the new information

from this work is helpful in understanding the mechanism of starch acid hydrolysis. For the waxy starch, the endo-corrosion pattern is the key to the degradation behavior. Specifically, the acid would degrade the amylopectin molecule by the cleavage of the α-(1→6) branch points in the amorphous zones, leading to the quick degradation of the lamellar structure. For the G80 starch, as the exo-corrosion pattern is the main degradation type, the lamellar structure could keep its origin form in the granule interior. Moreover, for G80, the lamellar peak intensity and crystallinity were increased with the increased acid hydrolysis time, However, the special molecular structure that is responsible for the acid resistance of G80 is worth further investigation. TGA results confirmed the molecular weight degradation of starch during acid hydrolysis.

Conflict of interest

The authors declare that there is no conflict of interests regarding the publication of this paper.

Acknowledgments

The authors from China would like to acknowledge the research funds NFSC (No. 31301554) and GNSF (No. 2015A030313428).

References

Blazek, J., & Gilbert, E. P. (2011). Application of small-angle X-ray and neutron scattering techniques to the characterisation of starch structure: A review. *Carbohydrate Polymers, 85*(2), 281-293.

Blennow, A., Hansen, M., Schulz, A., Jorgensen, K., Donald, A. M., & Sanderson, J. (2003). The molecular deposition of transgenically modified starch in the starch granule as imaged by functional microscopy. *Journal of Structural Biology, 143*(3), 229-241.

Chen, P., Wang, K., Kuang, Q., Zhou, S., Wang, D., & Liu, X. (2016). Understanding how the aggregation structure of starch affects its gastrointestinal digestion rate and extent. *International Journal of Biological Macromolecules, 87*, 28-33.

Chen, P., Yu, L., Simon, G., Petinakis, E., Dean, K., & Chen, L. (2009). Morphologies and

microstructures of cornstarches with different amylose-amylopectin ratios studied by confocal laser scanning microscope. *Journal of Cereal Science, 50*(2), 241-247.

Chen, P., Yu, L., Simon, G. P., Liu, X., Dean, K., & Chen, L. (2011). Internal structures and phase-transitions of starch granules during gelatinization. *Carbohydrate Polymers, 83*(4), 1975-1983.

Chung, Y.-L., & Lai, H.-M. (2006). Molecular and granular characteristics of corn starch modified by HCl-methanol at different temperatures. *Carbohydrate Polymers, 63*(4), 527-534.

Dhital, S., Warren, F. J., Zhang, B., & Gidley, M. J. (2014). Amylase binding to starch granules under hydrolysing and non-hydrolysing conditions. *Carbohydrate Polymers, 113*, 97-107.

Fan, D., Wang, L., Ma, S., Ma, W., Liu, X., Huang, J., Zhao, J., Zhang, H., & Chen, W. (2013). Structural variation of rice starch in response to temperature during microwave heating before gelatinisation. *Carbohydrate Polymers, 92*(2), 1249-1255.

Frost, K., Kaminski, D., Kirwan, G., Lascaris, E., & Shanks, R. (2009). Crystallinity and structure of starch using wide angle X-ray scattering. *Carbohydrate Polymers, 78*(3), 543-548.

Gérard, C., Colonna, P., Buléon, A., & Planchot, V. (2002). Order in maize mutant starches revealed by mild acid hydrolysis. *Carbohydrate Polymers, 48*(2), 131-141.

Genkina, N. K., Kiseleva, V. I., & Noda, T. (2009). Comparative investigation on acid hydrolysis of sweet potato starches with different amylopectin chain-length. *Starch/Staerke, 61*(6), 321-325.

Goderis, B., Reynaers, H., Koch, M. H. J., & Mathot, V. B. F. (1999). Use of SAXS and linear correlation functions for the determination of the crystallinity and morphology of semi-crystalline polymers. Application to linear polyethylene. *Journal of Polymer Science Part B: Polymer Physics, 37*(14), 1715-1738.

Huber, K. C., & BeMiller, J. N. (1997). Visualization of Channels and Cavities of Corn and Sorghum Starch Granules. *Cereal Chemistry, 74*(5), 537-541.

Huber, K. C., & BeMiller, J. N. (2000). Channels of maize and sorghum starch granules. *Carbohydrate Polymers, 41*(3), 269-276.

Jane, J.-l., Wong, K.-s., & McPherson, A. E. (1997). Branch-structure difference in starches of A- and B-type X-ray patterns revealed by their Naegeli dextrins. *Carbohydrate Research, 300*(3), 219-227.

Jiang, H., Srichuwong, S., Campbell, M., & Jane, J.-l. (2010). Characterization of maize amylose-extender (ae) mutant starches. Part III: Structures and properties of the Naegeli dextrins. *Carbohydrate Polymers, 81*(4), 885-891.

Jiang, S., Liu, C., Han, Z., Xiong, L., & Sun, Q. (2016). Evaluation of rheological behavior of starch nanocrystals by acid hydrolysis and starch nanoparticles by self-assembly: A comparative study. *Food Hydrocolloids, 52*, 914-922.

Kim, H.-S., & Huber, K. C. (2008). Channels within soft wheat starch A- and B-type granules. *Journal of Cereal Science, 48*(1), 159-172.

Kim, H.-Y., Lee, J. H., Kim, J.-Y., Lim, W.-J., & Lim, S.-T. (2012). Characterization of nanoparticles prepared by acid hydrolysis of various starches. *Starch - Stärke, 64*(5), 367-373.

Kuang, Q., Xu, J., Liang, Y., Xie, F., Tian, F., Zhou, S., & Liu, X. (2017). Lamellar Structure Change of Waxy Corn Starch during Gelatinization by Time-resolved Synchrotron SAXS. *Food Hydrocolloids, 62*, 43-48.

Kuang, Q., Xu, J., Wang, K., Zhou, S., & Liu, X. (2016). Structure and digestion of hybrid Indica rice starch and its biosynthesis. *International Journal of Biological Macromolecules, 93, Part A*,

402-407.

Le Corre, D. b., Bras, J., & Dufresne, A. (2010). Starch Nanoparticles: A Review. *Biomacromolecules, 11*(5), 1139-1153.

Li, E., Hasjim, J., Dhital, S., Godwin, I. D., & Gilbert, R. G. (2011). Effect of a gibberellin-biosynthesis inhibitor treatment on the physicochemical properties of sorghum starch. *Journal of Cereal Science, 53*(3), 328-334.

Li, Z., Kong, X., Zhou, X., Zhong, K., Zhou, S., & Liu, X. (2016). Characterization of multi-scale structure and thermal properties of Indica rice starch with different amylose contents. *RSC Advances, 6*, 107491-107497.

Liu, X., Ma, H., Yu, L., Chen, L., Tong, Z., & Chen, P. (2014). Thermal-oxidative degradation of high-amylose corn starch. *Journal of Thermal Analysis and Calorimetry, 115*, 659-665.

Liu, X., Wang, Y., Yu, L., Tong, Z., Chen, L., Liu, H., & Li, X. (2013). Thermal degradation and stability of starch under different processing conditions. *Starch - Stärke, 65*(1 - 2), 48-60.

Liu, X., Yu, L., Liu, H., Chen, L., & Li, L. (2008). In situ thermal decomposition of starch with constant moisture in a sealed system. *Polymer Degradation and Stability, 93*(1), 260-262.

Liu, X., Yu, L., Liu, H., Chen, L., & Li, L. (2009). Thermal decomposition of corn starch with different amylose/amylopectin ratios in open and sealed systems. *Cereal Chemistry, 86*(4), 383-385.

Liu, X., Yu, L., Xie, F., Li, M., Chen, L., & Li, X. (2010). Kinetics and mechanism of thermal decomposition of cornstarches with different amylose/amylopectin ratios. *Starch - Stärke, 62*(3 - 4), 139-146.

Liu, X., Zhang, N., Yu, L., Zhou, S., Shanks, R., & Zheng, J. (2016). Imaging the phase of starch–gelatin blends by confocal Raman microscopy. *Food Hydrocolloids, 60*, 7-10.

Pan, D. D., & Jane, J.-l. (2000). Internal Structure of Normal Maize Starch Granules Revealed by Chemical Surface Gelatinization. *Biomacromolecules, 1*(1), 126-132.

Qiao, D., Yu, L., Liu, H., Zou, W., Xie, F., Simon, G., Petinakis, E., Shen, Z., & Chen, L. (2016). Insights into the hierarchical structure and digestion rate of alkali-modulated starches with different amylose contents. *Carbohydrate Polymers, 144*, 271-281.

Song, W., Janaswamy, S., & Yao, Y. (2010). Structure and in Vitro Digestibility of Normal Corn Starch: Effect of Acid Treatment, Autoclaving, and β-Amylolysis. *Journal of Agricultural and Food Chemistry, 58*(17), 9753-9758.

Teng, A., Witt, T., Wang, K., Li, M., & Hasjim, J. (2016). Molecular rearrangement of waxy and normal maize starch granules during in vitro digestion. *Carbohydrate Polymers, 139*, 10-19.

Tran, T. T. B., Shelat, K. J., Tang, D., Li, E., Gilbert, R. G., & Hasjim, J. (2011). Milling of Rice Grains. The Degradation on Three Structural Levels of Starch in Rice Flour Can Be Independently Controlled during Grinding. *Journal of Agricultural and Food Chemistry, 59*(8), 3964-3973.

Wang, K., Hasjim, J., Wu, A. C., Henry, R. J., & Gilbert, R. G. (2014). Variation in Amylose Fine Structure of Starches from Different Botanical Sources. *Journal of Agricultural and Food Chemistry, 62*(19), 4443-4453.

Wang, S., Blazek, J., Gilbert, E., & Copeland, L. (2012). New insights on the mechanism of acid degradation of pea starch. *Carbohydrate Polymers, 87*(3), 1941-1949.

Wang, S., & Copeland, L. (2015). Effect of Acid Hydrolysis on Starch Structure and Functionality: A Review. *Critical Reviews in Food Science and Nutrition, 55*(8), 1081-1097.

Wang, Y. J., Truong, V. D., & Wang, L. (2003). Structures and rheological properties of corn starch as affected by acid hydrolysis. *Carbohydrate Polymers, 52*(3), 327-333.

Witt, T., Gidley, M. J., & Gilbert, R. G. (2010). Starch Digestion Mechanistic Information from the Time Evolution of Molecular Size Distributions. *Journal of Agricultural and Food Chemistry, 58*, 8444-8452.

Wu, A. C., Morell, M. K., & Gilbert, R. G. (2013). A Parameterized Model of Amylopectin Synthesis Provides Key Insights into the Synthesis of Granular Starch. *PLoS ONE, 8*(6), e65768.

Xie, F. W., Yu, L., Su, B., Liu, P., Wang, J., Liu, H. S., & Chen, L. (2009). Rheological properties of starches with different amylose/amylopectin ratios. *Journal of Cereal Science, 49*(3), 371-377.

Xu, J., Kuang, Q., Wang, K., Zhou, S., Wang, S., Liu, X., & Wang, S. (2017). Insights into molecular structure and digestion rate of oat starch. *Food Chemistry, 220*, 25-30.

Yang, J., Liang, Y., & Han, C. C. (2015). Effect of crystallization temperature on the interactive crystallization behavior of poly(l-lactide)-block-poly(ethylene glycol) copolymer. *Polymer, 79*, 56-64.

Yang, J., Liang, Y., Luo, J., Zhao, C., & Han, C. C. (2012). Multilength Scale Studies of the Confined Crystallization in Poly(l-lactide)-block-Poly(ethylene glycol) Copolymer. *Macromolecules, 45*(10), 4254-4261.

Yang, Z., Gu, Q., Lam, E., Tian, F., Chaieb, S., & Hemar, Y. (2016). In situ study starch gelatinization under ultra-high hydrostatic pressure using synchrotron SAXS. *Food Hydrocolloids, 56*, 58-61.

Zavareze, E. d. R., & Dias, A. R. G. (2011). Impact of heat-moisture treatment and annealing in starches: A review. *Carbohydrate Polymers, 83*(2), 317-328.

Zhang, N., Liu, H., Yu, L., Liu, X., Zhang, L., Chen, L., & Shanks, R. (2012). Developing gelatin–starch blends for use as capsule materials. *Carbohydrate Polymers, 92*(1), 455–461.

Zhang, N., Liu, X., Yu, L., Shanks, R., Petinaks, E., & Liu, H. (2013). Phase composition and interface of starch-gelatin blends studied by synchrotron FTIR micro-spectroscopy. *Carbohydrate Polymers, 95*(20), 649–653.

Tables and Figures

Tables and Figures

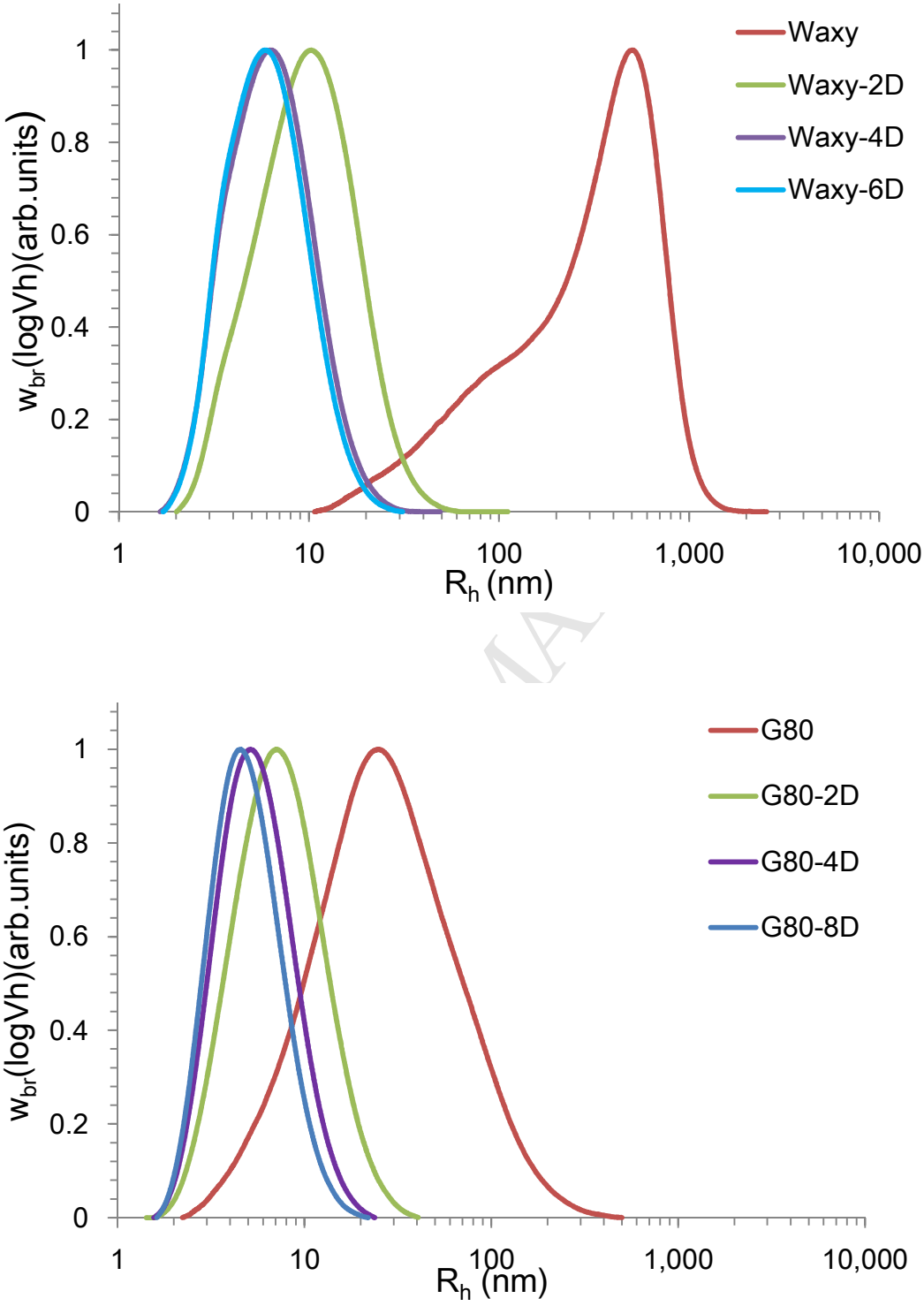

Fig.1. SEC weight distributions of the whole (fully-branched) native and acid-hydrolyzed starches (upper: waxy maize starch; bottom: G80 maize starch).

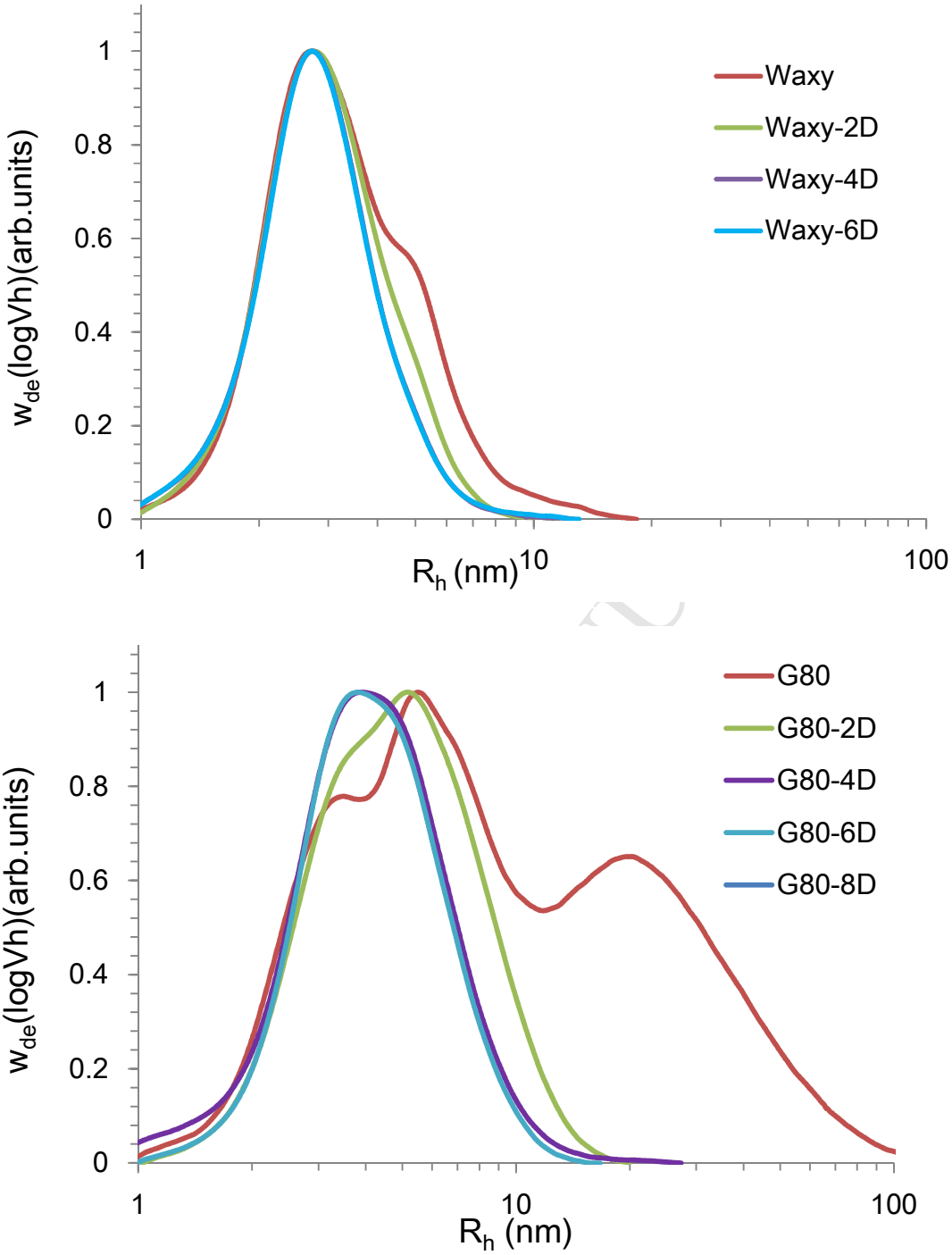

Fig.2. SEC weight distributions of the debranched native and acid-hydrolyzed starches (upper: waxy maize starch; bottom: G80 maize starch).

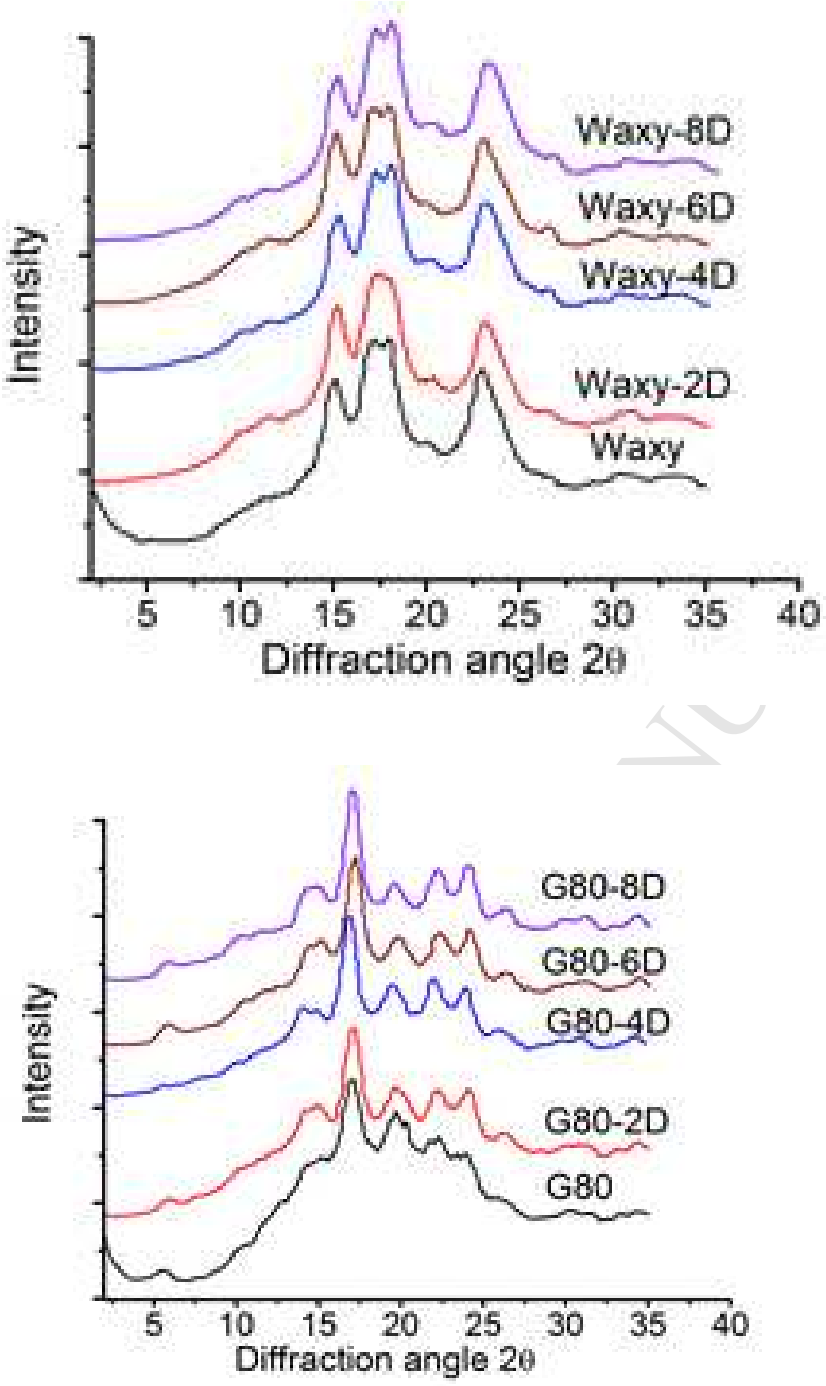

Fig.3. X-ray diffraction spectra for the native and acid-hydrolyzed starches (upper: waxy maize starch; bottom: G80 maize starch).

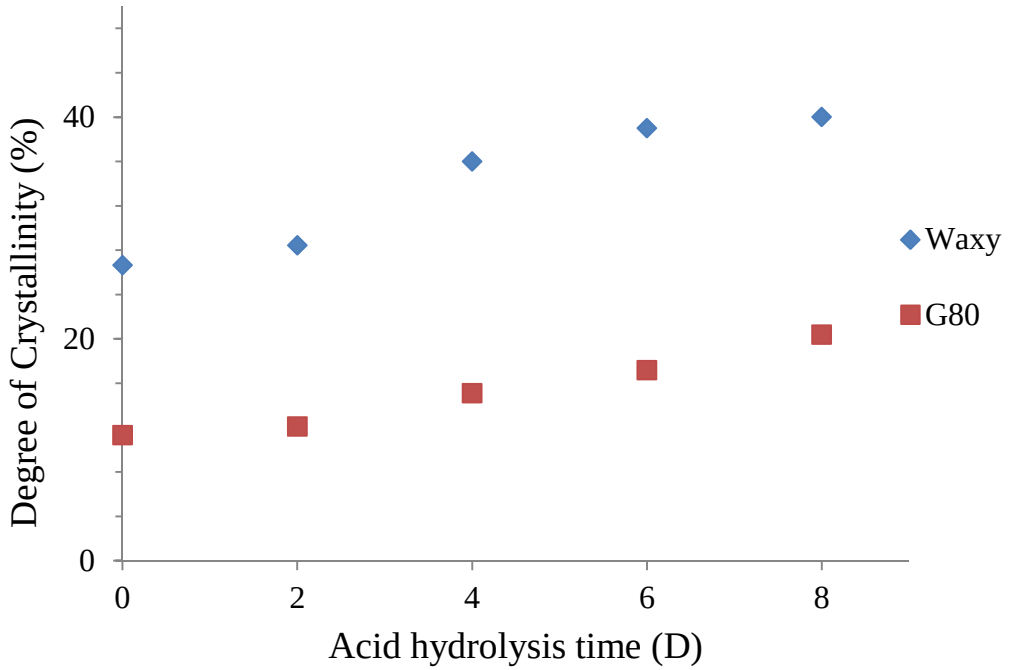

Fig.4. Effect of the acid hydrolysis time on the degree of crystallinity of waxy and G80 maize starches.

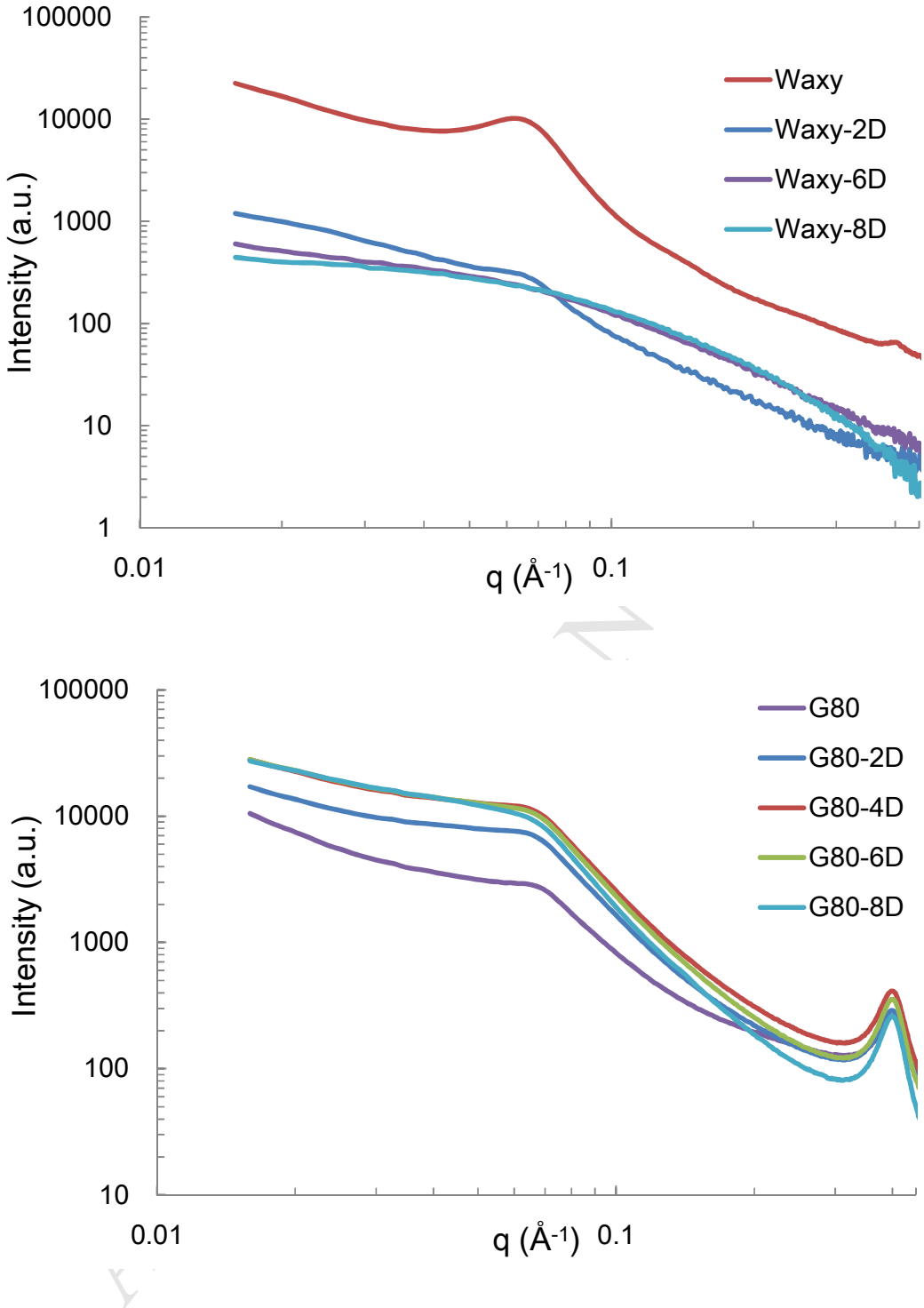

Fig.5. Double-logarithmic SAXS patterns for the native and acid-hydrolyzed starches (Upper: waxy maize starch; Lower: G80 maize starch).

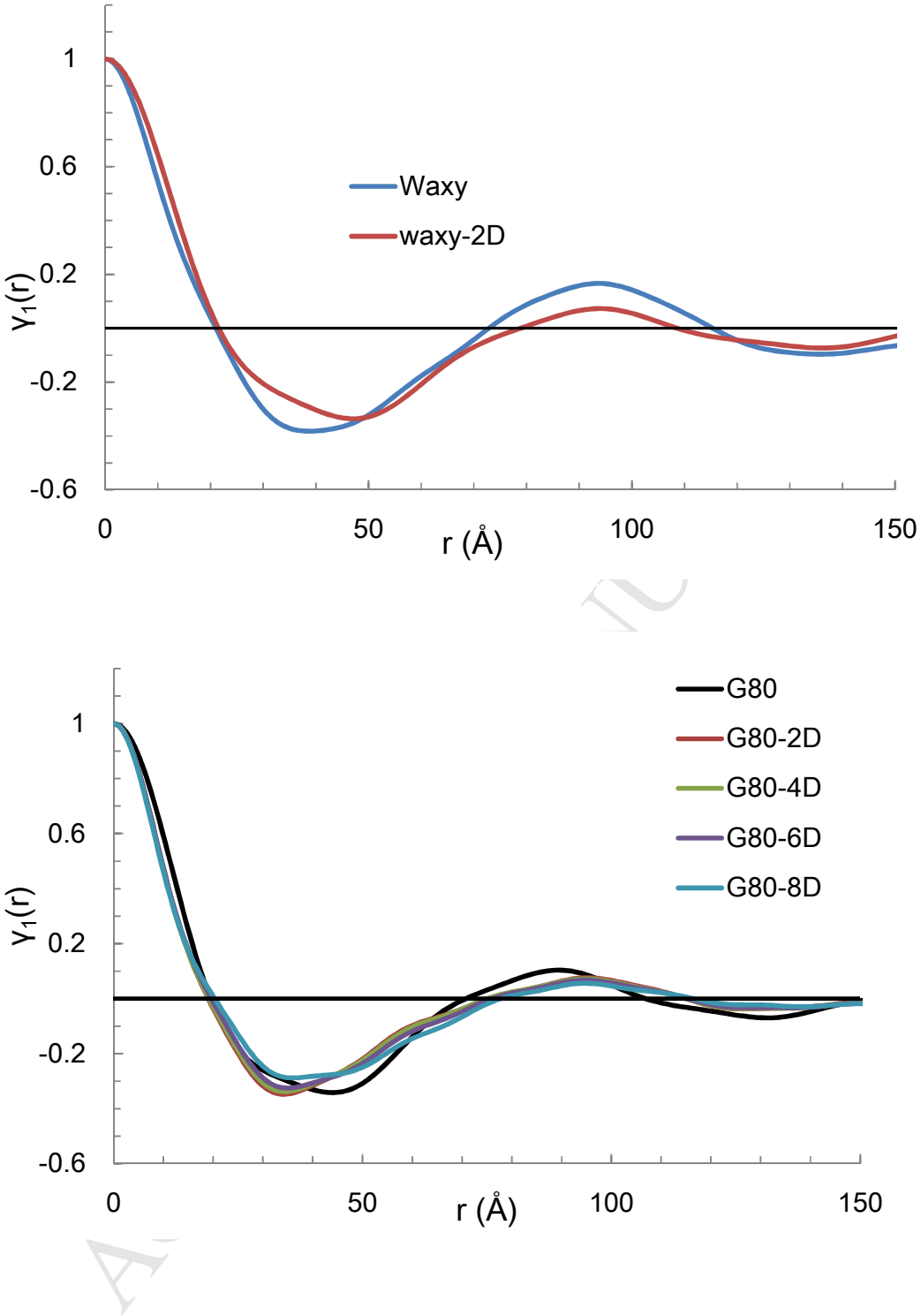

Fig.6. Normalized 1D-correlation function for the native and acid-hydrolyzed starches (upper: waxy maize starch; bottom: G80 maize starch).

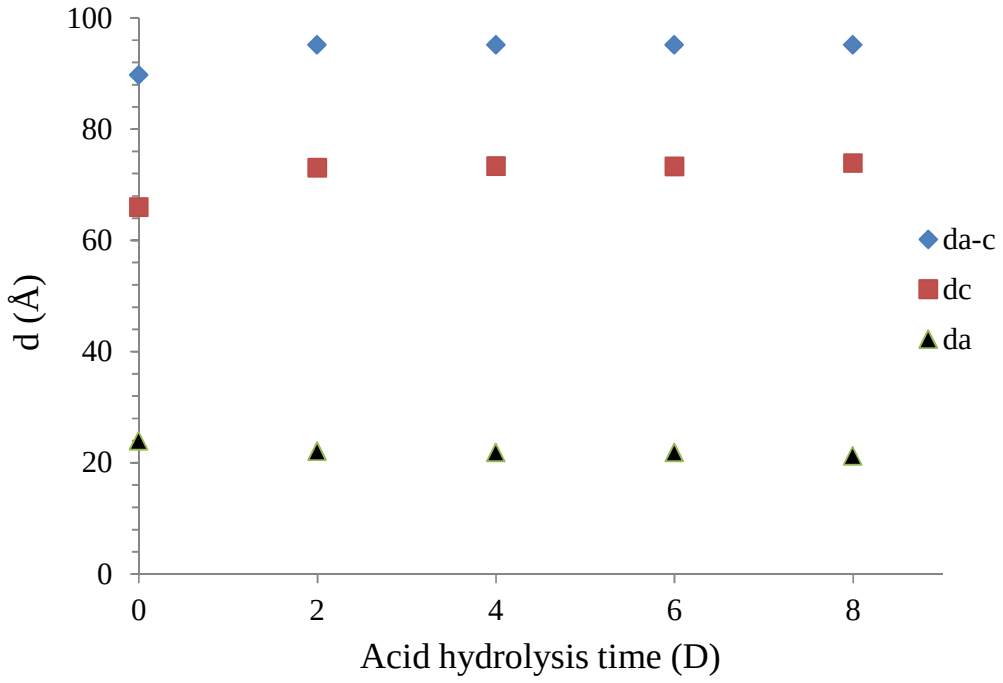

Fig.7. Changes in the long period ($d_{a\text{-}c}$), thickness of amorphous layer (d_a) and thickness of crystalline layer (d_c) as a function of acid hydrolysis time for G80 maize starch.

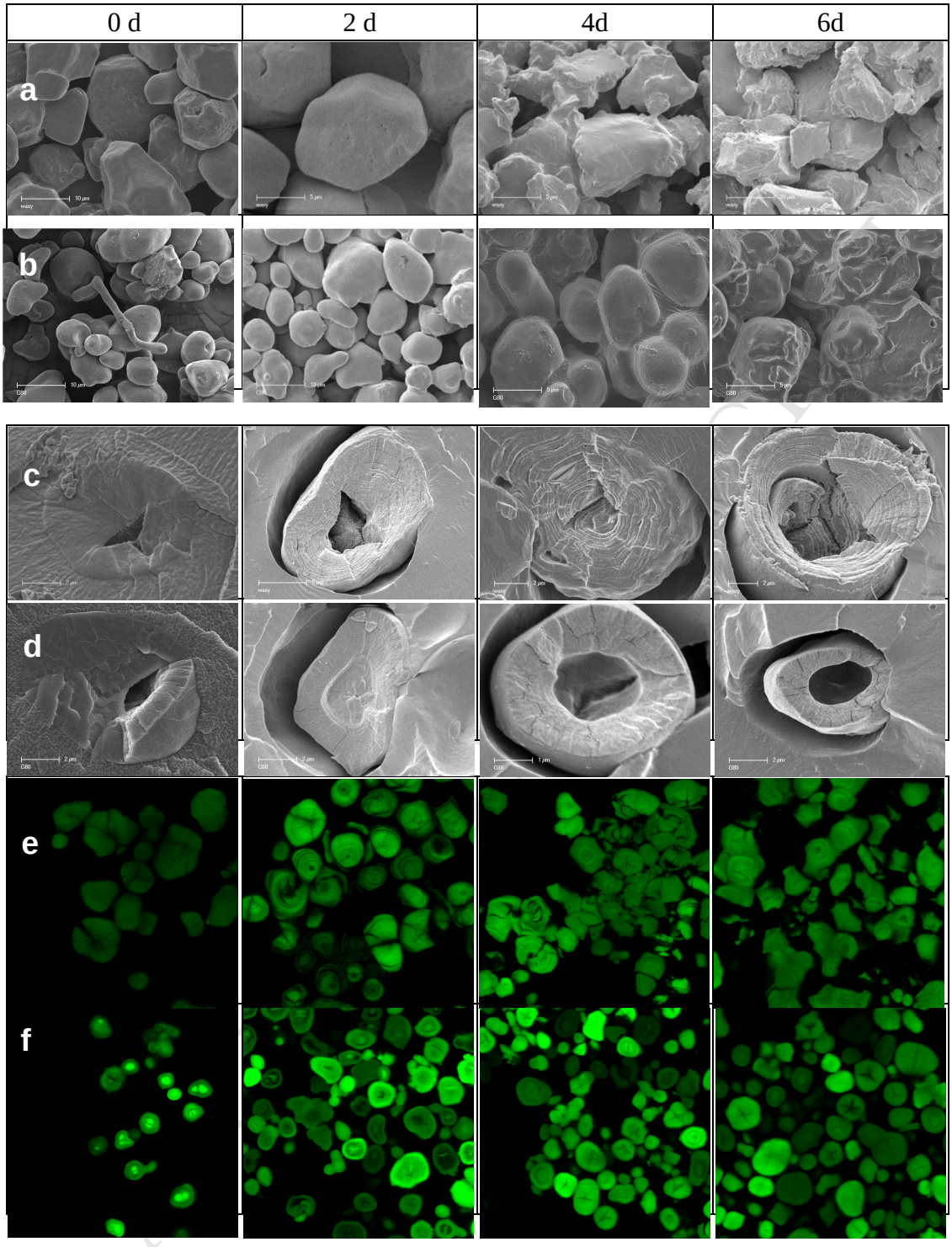

Fig.8 SEM and CLSM images of the different starches with different acid hydrolysis times: (a) (c) and (e) shows waxy maize starch; and (b), (d) and (f) display G80 maize starch.

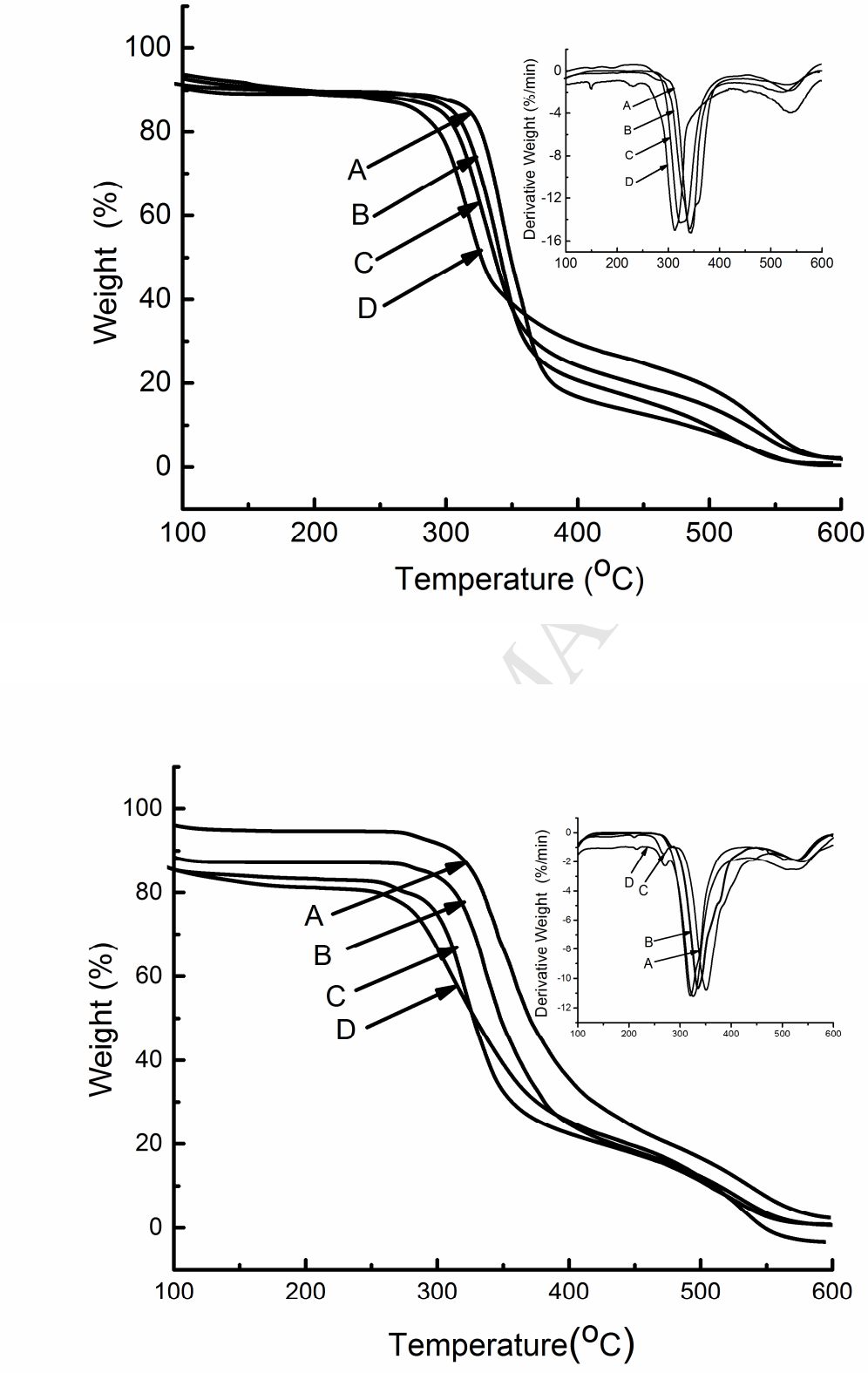

Fig.9. Thermal decomposition of the waxy (upper) and G80 (bottom) maize starches with different acid hydrolysis times: A: 0 day; B: 3 days; C: 6 days; D:12 days.

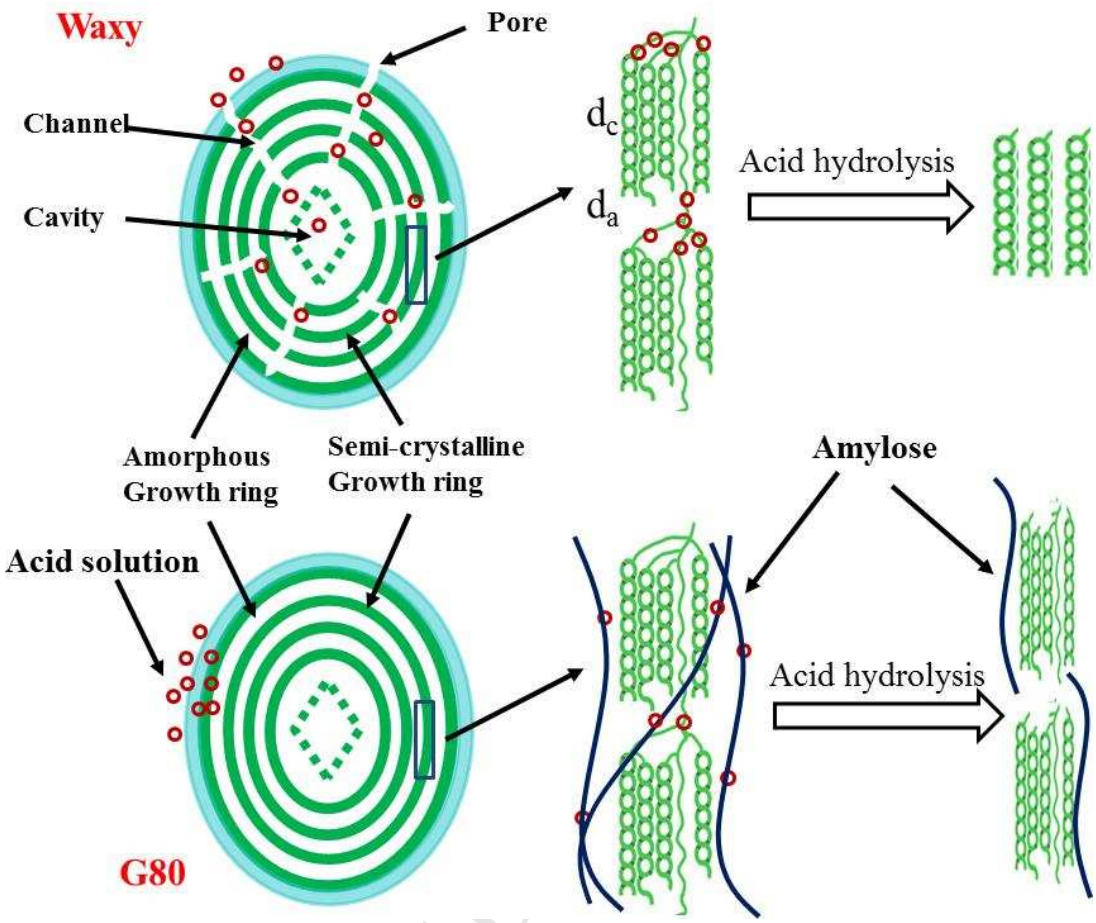

Fig.10. The proposed mechanism of starch acid hydrolysis

Highlights

1. Multi-scale structural changes of starch granules during acid hydrolysis were investigated.
2. Acid hydrolysis decreased the starch molecular size to a stable value
3. Acid disrupted the waxy starch lamellar structure effectively
4. Two different degradation pattern were observed in starch granules
5. Thermal decomposition temperature of acid-hydrolyzed starch became lower